Electron energetics in the expanding solar wind via Helios observations

Štěpán Štverák,[1,2] Pavel M. Trávníček,[3,1,2] and Petr Hellinger[1,2]

Abstract. We present an observational analysis of electron cooling/heating rates in the fast and slow solar wind between 0.3 and 1 AU. We fit electron velocity distribution functions acquired in situ by Helios 1 and 2 spacecraft by a three component (core-halo-strahl) analytical model. The resulting radial profiles of macroscopic characteristics (density, temperatures and heat fluxes) are employed to examine properties of theoretical energy balance equations and to estimate external cooling/heating terms. Our analysis indicates that in contrast to solar wind protons the electrons do not require important heating mechanisms to explain the observed temperature gradients. The electron heating rates are actually found to be negative for both the slow and fast solar wind, namely due to the significant degradation of the electron heat flux with increasing radial distance from the Sun. Cooling mechanisms acting on electrons are found to be significantly stronger in the slow wind than in the fast wind streams.

1. Introduction

Based on currently available in situ observations the overall electron energetics in the expanding solar wind is poorly understood. The processes responsible for driving electron properties still need to be better established on the theoretical background. Since the observed electron temperature gradients in the solar wind do not correspond to theoretical adiabatic predictions the question arises whether any external heating is required and what are the mechanisms responsible for driving the non-adiabatic behavior. So far only few studies investigated the empirical heating and/or cooling rates required to support the observed electron temperature and heat flux gradients. *Pilipp et al.* [1990] provided a detailed analysis of the original Helios 1 and 2 data sets covering also the basic aspects of the electron energetics. They concluded that both the heating and cooling take place depending on the solar wind properties. While a rather significant cooling was observed in the slow solar wind streams a need for low to moderate heating was identified in the fast streams. Later on *Hu et al.* [1997] examined the energy requirements of the fast solar wind by means of a two-fluid model where a need of an efficient electron cooling was recognized in order to match the high electron temperatures near the corona. More recently *Cranmer et al.* [2009] published similar but rather simplified analysis compared to *Pilipp et al.* [1990] by extending the Helios data set with Ulysses in-ecliptic observations restricted to fast wind streams only. Again, they found non negligible electron heating, however, the combined data set introduced some additional features which made the interpretation of the results difficult. The present paper aims to review and further extend our understanding of the electron energetics in the solar wind analyzing its radial trends between 0.3 and 1 AU based on the Helios data set only.

In the simplest approximation of an isotropic plasma the energy balance equation for a single plasma species, as de-

rived from the general Boltzmann equation, reads as

$$
nk_B \left(\frac{\partial}{\partial t} + \mathbf{u} \cdot \nabla \right) T = -\frac{2}{3} nk_B T \nabla \cdot \mathbf{u} - \nabla \cdot (q\mathbf{b})
$$
$$
+ nk_B \left(\frac{\partial T}{\partial t} \right)_c + Q \qquad (1)
$$

where n is the particle number density, T is the total temperature, $\mathbf{u}$ is the bulk speed, q is the heat flux (all these quantities belongs to a given plasma species), $\mathbf{b} = \mathbf{B}/|\mathbf{B}|$ with $\mathbf{B}$ being the magnetic field vector, and k_B is the Boltzmann constant (note that all symbols are defined in Appendix A). The last term Q does not result directly from the integration of the Boltzmann equation but represents any external heating or cooling mechanisms which may be present. Assuming a purely radial adiabatic expansion of electrons in thermal equilibrium equation (1) predicts a theoretical temperature radial profile of $T \propto R^{-4/3}$. However the solar wind electrons with their mean free path being comparable to local characteristic scales are neither fully collisional nor completely collisionless and are also typically found to exhibit many non-thermal features. Consequently, observed electron temperature gradients span from almost adiabatic to even nearly isothermal radial profiles [see, e.g., *Ogilvie and Scudder*, 1978; *Feldman et al.*, 1979; *Pilipp et al.*, 1990; *Scime et al.*, 1994; *Issautier et al.*, 1998; *Maksimovic et al.*, 2000]. By a simple inspection of equation (1) there are two internal mechanisms which, besides the effect of the expansion, may influence the observed temperature profiles. In a closed system either the dissipation of the heat flux and/or the Coulomb collisions may effectively contribute to the electron energy balance. However, if both the heat flux and collisional effects are not strong enough, the energy balance may require some external heating/cooling rates (Q). A fundamental question then arises whether the observed non-adiabatic evolution of solar wind electrons is due to some external heating mechanisms or it is simply caused by the nature of the electron characteristic properties (or it is a combination of both).

A natural external source of energy for the electron heating represents the solar wind turbulence/wave activity. The heating properties of the weakly collisional solar wind plasma turbulence is however not understood. The fluctuating electromagnetic field spectra in the solar wind have their largest amplitudes at wavelengths very long compared to the electron (and even ion) scales. At such wavelengths,

[1]Astronomical Institute, CAS, Prague, Czech Republic.
[2]Institute of Atmospheric Physics, CAS, Prague, Czech Republic.
[3]Space Sciences Laboratory, University California Berkeley, California, USA.

collisionless damping is very weak; the weakness of wave-particle interactions in this regime implies that MHD models for turbulence are appropriate [cf. *Bruno and Carbone*, 2013, and references therein]. It is generally assumed that an MHD turbulent cascade leads to the transfer of the injected energy to shorter scales and heats charged particles (i.e., shape their velocity distributions). Still the solar wind turbulence is now understood only on a phenomenological level with large uncertainties concerning the cascade properties at small scales and the properties of dissipation processes and their impact on the energetics and velocity distribution functions of the different species. The properties of turbulence become even more complex due to the solar wind expansion. The expansion leads to a decrease of fluctuating amplitudes and changes the characteristic particle scales in the vicinity of which the turbulent heating is expected.

In terms of internal heating and energy exchange mechanisms electrons, unlike solar wind protons and other minor ions, typically exhibit a rather strong heat flux and also the effect of Coulomb collisions can not be completely neglected. Besides the thermal core population and the suprathermal halo tails which are both present at all pitch angles, the electron velocity distribution functions almost permanently exhibit a magnetic field aligned beam-like component mostly oriented in the anti-sunward direction, the so-called strahl [see, e.g., *Montgomery et al.*, 1968; *Feldman et al.*, 1975; *Rosenbauer et al.*, 1977; *Pilipp et al.*, 1987a]. The electron heat flux is then provided by the relative drift between the strahl and the core and halo populations. Assuming collisionless electrons and no dissipation of the electron heat flux *Scime et al.* [1994] have shown that for a free expansion along a spiral magnetic field the heat flux will fall off as R^{-2} for a radial magnetic field and as $\sim R^{-1}$ at larger radial distances where the magnetic field becomes almost transverse. However, observations from the Helios and Ulysses spacecraft show that the electron heat flux decreases with the radial distance considerably steeper. Observations of *Pilipp et al.* [1990] or *Scime et al.* [1994] give almost $q \propto R^{-3}$; such fast degradation of the electron heat flux far beyond the free streaming approach indicates that some dissipative mechanisms effectively reduce the heat flux along the expansion and potentially heat the electrons. The dissipation can be provided via the wave-particle interactions represented namely by various heat flux instabilities [*Gary et al.*, 1975, 1994, 1999] as it is also indicated by Cluster observations recently reported by *Lacombe et al.* [2014]. Moreover, kinetic simulations performed by *Landi et al.* [2012, 2014] have shown that also Coulomb collisions by themselves can effectively control the electron heat flux properties and thus contribute to the electron thermal evolution.

On top of the important non-thermal heat flux properties the solar wind electrons also typically exhibit non-negligible temperature anisotropies: the parallel temperature $T_\parallel$ usually exceeds the perpendicular temperature $T_\perp$ by a factor of 1.2 [*Feldman et al.*, 1975; *Pilipp et al.*, 1987b]. The observed temperature anisotropies are equally indicated to be constrained by kinetic instabilities [cf., *Štverák et al.*, 2008, and references therein] and electron-electron Coulomb collisions [*Salem et al.*, 2003]. The kinetic instabilities related to the temperature anisotropies and also electron-electron Coulomb collisions therefore can play an important role in the overall electron energetic evolution. In equation (1), however, we assume isotropic electrons with a single temperature $T = T_\perp = T_\parallel$. For a more realistic description of the true solar wind state the anisotropic approach shall be adopted where we derive similar equations describing the evolution of the parallel and perpendicular temperature separately, again by taking the corresponding moments of the Boltzmann equation. For anisotropic electrons we obtain [cf., *Barakat and Schunk*, 1982; *Marsch et al.*, 1983;

Hellinger et al., 2011]

$$nk_B \left(\mathbf{u} \cdot \nabla\right) T_\parallel = -2nk_B(\nabla_\parallel \cdot \mathbf{u})T_\parallel - \nabla \cdot (q_\parallel \mathbf{b}) + 2q_\perp \nabla \cdot \mathbf{b}$$
$$+ nk_B \left(\frac{\partial T_\parallel}{\partial t}\right)_c + Q_\parallel \qquad (2)$$

$$nk_B \left(\mathbf{u} \cdot \nabla\right) T_\perp = -nk_B T_\perp \nabla_\perp \cdot \mathbf{u} - \nabla \cdot (q_\perp \mathbf{b}) - q_\perp \nabla \cdot \mathbf{b}$$
$$+ nk_B \left(\frac{\partial T_\perp}{\partial t}\right)_c + Q_\perp \qquad (3)$$

where the subscripts $\parallel$ and $\perp$ represent the parallel and perpendicular components of the quantities wrt. the magnetic field direction (again all the symbols are defined in Appendix A). The terms $Q_\parallel$ and $Q_\perp$, likewise in equation (1), represent external heating/cooling mechanisms acting in the two corresponding directions. Note that in comparison to equation (1), equations (2)-(3) with no collisions, heat flux dissipation, and neither other cooling/heating mechanisms will lead in a simplified geometry where both the expansion and magnetic field are purely radial to the temperature profiles with $T_\perp \propto r^{-2}$ and $T_\parallel = cnts$. Such profiles are in fact compliant to a more general double adiabatic prediction where $T_\perp \propto B$ and $T_\parallel \propto n^2/B^2$ [cf., *Chew et al.*, 1956] which is, however, valid for supersonic populations only [*Schulz and Eviatar*, 1973]. For subsonic electrons *Landi et al.* [2012] have shown that simply applying Liouville's theorem with energy and magnetic moment conservation and without collisions will lead to the formation of slightly modified temperature profiles (see Figure 2 therein) where the perpendicular cooling is compensated by parallel heating and bulk flow acceleration.

The main goal of the present paper is to evaluate equations (1)-(3) by means of the in situ observations and assess the importance of the individual terms, in particular the heating/cooling rates represented by external mechanisms (Q). The full procedure of the data analysis and obtained results are described in section 2. We start with the description of the Helios 1 and 2 data sets in subsection 2.1. In subsection 2.2 we derive from the data set the mean radial profiles of the characteristic electron properties to construct a kind of their average solar wind representative which we subsequently use to evaluate equations (1)-(3) and to quantify the heating rates in subsection 2.3. The obtained results are then discussed in a general context in section 3 and the summary conclusions are given in section 4. Any symbols used throughout the whole paper and complementary data analysis methods are defined in Appendix A and B respectively.

2. Data analysis

2.1. Data set

We analyze the electron velocity distribution functions acquired by the Helios 1 and Helios 2 spacecraft. The data set was collected in the period between 1975 and 1978 around the solar minimum at the cross over from solar cycle 20 to 21. The heliocentric radial range of the data set spans from 0.3 up to 1 AU within the ecliptic plane.

On both Helios 1 and 2 spacecraft the electron velocity distributions were acquired with almost identical one dimensional electron analyzers. The Helios probes were spinning spacecraft with the spin axis oriented perpendicular to the ecliptic plane. A full 2π cut of the electron distribution was acquired by the use of the spacecraft rotation with the time resolution of about 40 s. The two dimensional cuts are divided into eight uniform angular bins spaced $45°$ apart with a polar and azimuthal field of view of $19°$ and $28.1°$ respectively. The full energy range covered by the instrument in
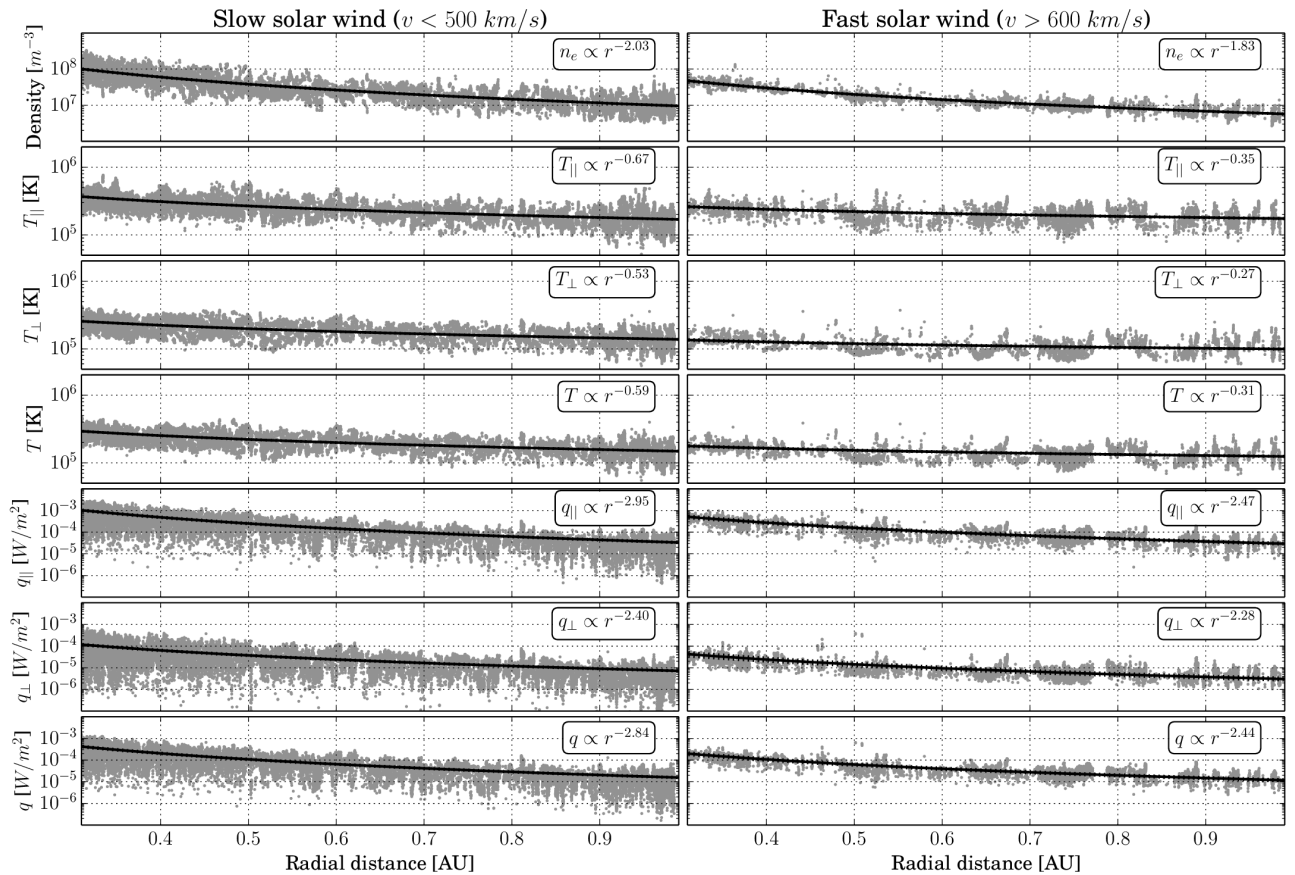
Figure 1. Empirical power-law radial profiles as derived from the Helios 1 and 2 electron measurements. The left and right panels show the profiles for the slow and fast wind respectively. Estimated electron characteristics for individual data samples are indicated as gray dots and the solid black lines represent the resulting fitted profiles. Due to large number of data points the errors of the mean profiles are typically of the order of line thickness. The confidence intervals shown with black dotted lines are therefore barely visible for the electron heat flux in the fast wind only.

each of the eight angular bins was distributed between 0.5 and 1658 eV in 32 energy channels. For the detailed description of the instrument performance and data processing see *Schwenn et al.* [1975] or *Rosenbauer et al.* [1977]. The measured electron data are further described in *Pilipp et al.* [1984].

In order to well recover the properties of all three distinct electron populations, i.e., the core, halo, and strahl with the 2-D cut of the electron distribution we adopted the sample preselection rules from *Štverák et al.* [2009]. First only those measurements for which the local interplanetary magnetic field is close to be perpendicular with the spacecraft spin axis, thus in the field of view of the electron analyzer, are processed for further analysis. This ensures that any temperature anisotropies with respect to the magnetic field are captured in the measured samples. In addition we also require the magnetic field vector to be well aligned to the axis of one of the eight instrument angular bins so that the bulk of an even narrow field aligned strahl population is always well resolved by the detector. The two conditions in general guarantee to have a good estimate of the electron distribution in the $(v_\perp, v_\parallel)$ plane, where the directions $\perp$ and $\parallel$ are with respect to the local magnetic field vector. The final preselected data set contains roughly 230 thousand of individual data samples.

2.2. Empirical radial profiles

The evaluation of equations (1) to (3) requires the knowledge of basic macroscopic characteristics of the given plasma species, i.e., in our case the characteristics of the electron population. For our analysis we have employed solar wind electron properties as derived in *Štverák et al.* [2009]. The measured electron distributions are transformed to the solar wind frame and corrected with respect to the estimated spacecraft potential effect using a calibration to the measured ion densities and bulk velocities [*Pilipp et al.*, 1984]. The corrected distributions are consequently fitted with a full analytical model where the core population is described as a drifting bi-Maxwellian, the supra-thermal tails of the halo are expressed using a truncated bi-Kappa distribution, and finally the strahl beam-like population is represented with a bi-Kappa distribution depressed in the thermal range of the core electrons. Detailed analytical description of the model distribution functions is given by equations (1)-(10) in *Štverák et al.* [2009]. Since the model is non-linear in most of its parameters the fitting algorithm implements the Levenberg-Marquardt method [*Marquardt*, 1963]. The final parameters are adjusted in several consecutive steps in order to well separate the three distinct components, i.e., the core, halo, and strahl population. The required electron characteristics, i.e., the number density (n), parallel and perpendicular temperatures ($T_\parallel$ and $T_\perp$, respectively), and parallel and perpendicular components of the electron heat flux ($q_\parallel$ and $q_\perp$, respectively), are derived numerically as the corresponding moments of the model distribution function (see Appendix A for exact definitions).

Instead of substituting into equations (1)-(3) directly the electron properties derived for individual data samples we first fit the observations as a function of the radial distance

Table 1. Empirical radial power-law profiles of mean electron properties in the slow and fast solar wind. The fitted parameters A and α are given together with their relative uncertainties.

Model	Fitted parameters			
radial profile	Slow wind		Fast wind	
$y = A(R/R_0)^\alpha$	A	α	A	α
$n\,[m^{-3}]$	9.32e+06 $\pm$ 1.70%	-2.03 $\pm$ 0.95%	5.61e+06 $\pm$ 1.88%	-1.83 $\pm$ 1.49%
$T_{\parallel}\,[K]$	1.68e+05 $\pm$ 0.43%	-0.67 $\pm$ 0.86%	1.74e+05 $\pm$ 0.98%	-0.35 $\pm$ 4.78%
$T_{\perp}\,[K]$	1.37e+05 $\pm$ 0.37%	-0.53 $\pm$ 0.94%	9.92e+04 $\pm$ 1.07%	-0.27 $\pm$ 6.84%
$T\,[K]$	1.48e+05 $\pm$ 0.36%	-0.59 $\pm$ 0.83%	1.24e+05 $\pm$ 0.92%	-0.31 $\pm$ 5.09%
$q_{\parallel}\,[Wm^{-2}]$	3.23e-05 $\pm$ 3.90%	-2.95 $\pm$ 1.35%	2.86e-05 $\pm$ 7.58%	-2.47 $\pm$ 3.33%
$q_{\perp}\,[Wm^{-2}]$	7.05e-06 $\pm$ 3.57%	-2.40 $\pm$ 1.61%	2.97e-06 $\pm$ 13.08%	-2.28 $\pm$ 6.39%
$q\,[Wm^{-2}]$	1.52e-05 $\pm$ 3.80%	-2.84 $\pm$ 1.39%	1.15e-05 $\pm$ 7.97%	-2.44 $\pm$ 3.55%

from the Sun in order to get their mean radial profiles. The empirical profiles not only provide the evaluation of the energy balance equations as a single function of the radial distance but more importantly enable the estimation of required radial gradients which are otherwise very difficult to derive based on the direct in situ observations. For all empirical mean radial profiles we use a simple power-law function in the form

$$y(R) = A(R/R_0)^\alpha \qquad (4)$$

where A and α are the two free parameters and $R_0 = 1$ AU. We use a non-linear least square regression in order to estimate not only the free parameters but also their variance from the processed in situ observations. We further treat the two distinct solar wind populations, i.e., the slow and fast solar wind streams separately. As a slow solar wind stream we consider data samples with the proton bulk speed of the solar wind below 500 km/s and take the proton bulk speed of 600 km/s as the lower boundary for the fast solar wind data samples. The parameters A and α for resulting radial profiles of all basic solar wind properties in the slow and fast solar wind are given in Table 1 including the corresponding relative standard errors. The estimation of the errors in the fit parameters due to data uncertainties is described in the Appendix B. The individual fits of the power-law profiles are plotted over Helios measurements in Figure 1. In each panel of Figure 1 the data points are plotted with grey dots and the fitted profile with a solid black line. The confidence intervals are plotted with a pair of dotted lines, however, due to large number of data points and thus rather small relative error of the parameters, these intervals are mostly of the order of the line thickness.

2.3. Derived heating/cooling rates

In order to test the energy balance equations (1)-(3) for the electron population in the expanding solar wind we define the average heating rate Q as follows: for the isotropic approach we define the total heating rate Q to be

$$Q = Q_T + Q_q + Q_{C,ep} \qquad (5)$$

where the three terms on the right hand side are given by equation (1) as

$$
\begin{aligned}
Q_T &= nk_B \left(\mathbf{u} \cdot \nabla + \frac{2}{3}\nabla \cdot \mathbf{u} \right) T \\
Q_q &= \nabla \cdot (q\mathbf{b}) \\
Q_{C,ep} &= -nk_B \left(\frac{\partial T}{\partial t} \right)_c
\end{aligned} \qquad (6)
$$

so that the term Q_T corresponds to the heating rate as derived from the adiabatic expansion while the Q_q and $Q_{C,ep}$ terms quantify the energetic contributions of the internal

electron heat flux and Coulomb electron-proton collisions, respectively (n.b. electron-electron collisions do not contribute to the heating rate Q in the isotropic approach). All symbols on the right hand sides of equations (6) have the same meaning as in equation (1). With such definition of Q one can deduce that for resulting positive energization rates ($Q > 0$) the electrons are heated by an external source so that the temperature decreases with the radial distance slower than predicted for an adiabatic system. On the other hand a negative energization rate ($Q < 0$) implies an additional cooling of the electron population so that the temperature radial gradient becomes steeper than expected.

In the case of the anisotropic approach given by equations (2)-(3) we define a total average heating rate Q as

$$Q = (2Q_\perp + Q_\parallel)/3 \qquad (7)$$

where the parallel and perpendicular contributions are given similarly to equations (6) as

$$
\begin{aligned}
Q_\parallel &= Q_{\parallel,T} + Q_{\parallel,q} + Q_{\parallel,C} \\
Q_\perp &= Q_{\perp,T} + Q_{\perp,q} + Q_{\perp,C}
\end{aligned} \qquad (8)
$$

with

$$
\begin{aligned}
Q_{\parallel,T} &= nk_B \left((\mathbf{u} \cdot \nabla) + 2(\nabla_\parallel \cdot \mathbf{u}) \right) T_\parallel \\
Q_{\parallel,q} &= \nabla \cdot (q_\parallel \mathbf{b}) - 2q_\perp \nabla \cdot \mathbf{b} \\
Q_{\parallel,C} &= -nk_B \left(\frac{\partial T_\parallel}{\partial t} \right)_c
\end{aligned} \qquad (9)
$$

and

$$
\begin{aligned}
Q_{\perp,T} &= nk_B \left((\mathbf{u} \cdot \nabla) + (\nabla_\perp \cdot \mathbf{u}) \right) T_\perp \\
Q_{\perp,q} &= \nabla \cdot (q_\perp \mathbf{b}) + q_\perp \nabla \cdot \mathbf{b} \\
Q_{\perp,C} &= -nk_B \left(\frac{\partial T_\perp}{\partial t} \right)_c
\end{aligned} \qquad (10)
$$

In the right hand sides of equations (9) and (10) all terms have the same definition as in equations (2) and (3), respectively, and their corresponding definitions are again provided in Appendix A.

We evaluate equations (5) to (10) using mean radial profiles derived in the section 2.2 from the in situ observations (see Table 1) with the following assumptions. Any empirical profile of the solar wind speed derived on our data sample will be significantly biased by the two artificial cut-off velocities, i.e., 500 km/s and 600 km/s for the slow and fast solar wind respectively. For the mean solar wind speed $\mathbf{u}$ we therefore use rather a flat constant profile with empirical values of 400 km/s and 700 km/s in the case of slow and fast solar wind, respectively [cf., *Hellinger et al.*, 2011, 2013].
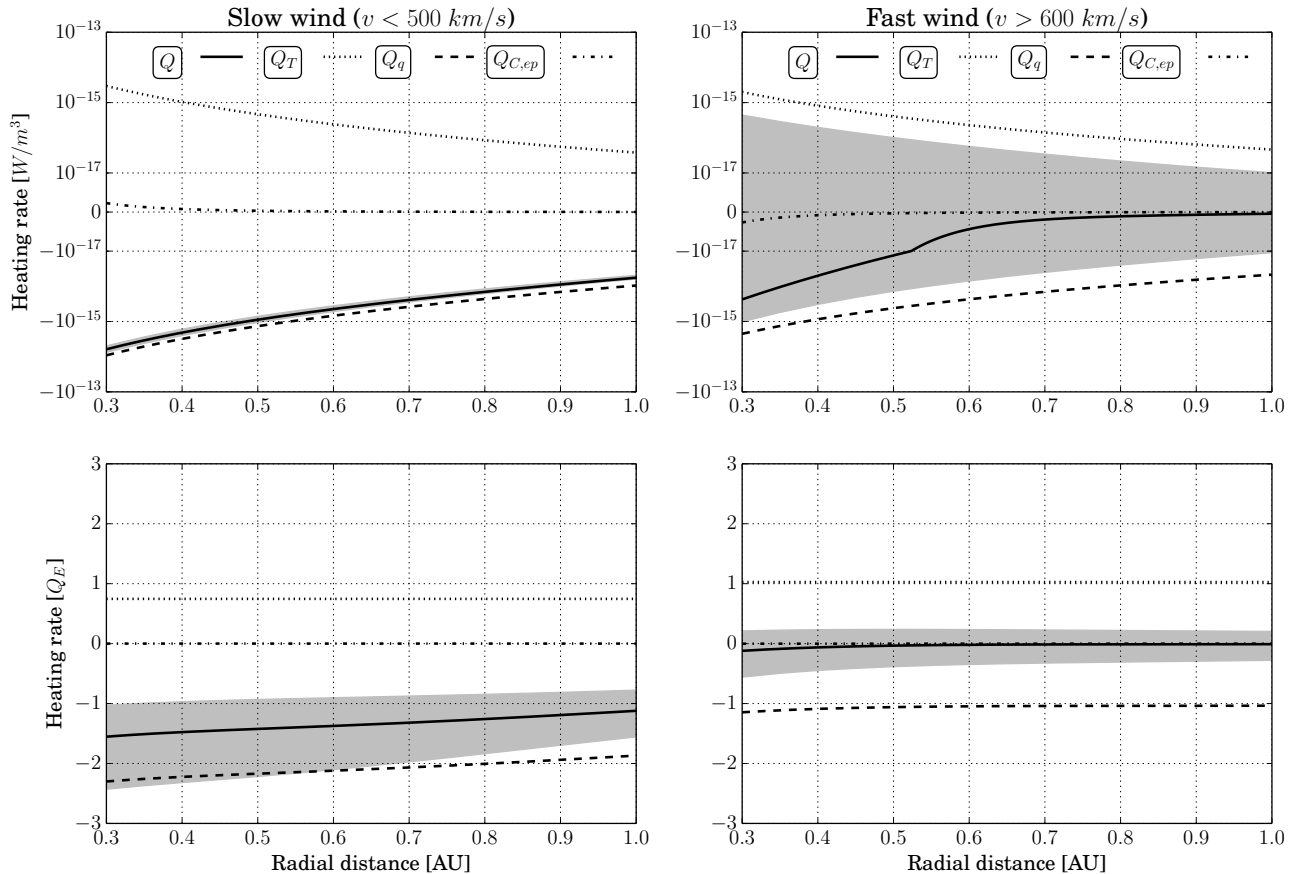
Figure 2. Individual terms of the isotropic energy balance equation for the slow (left panels) and fast (right panels) solar wind are shown as the function of the radial distance from the Sun. The three individual contributions Q_T, Q_q, Q_C (see eq. 6) and the total average rate Q are represented by dashed, dash-dotted, dotted, and solid lines, respectively. The y-axis correspond to the heating rates in W/m^3 (upper panels) and employs a symmetric logarithmic scale (with a small linear scale interval around zero). The lower panels show the heating rates normalized to the characteristic heating rate $Q_E = n k_B T u / R$. Grey shaded areas identify the 95% confidence intervals of the total heating rate Q as derived from the error analysis.

Indeed, such selection of solar wind speed profiles is well comparable also to our data set properties.

The magnetic field is assumed to follow the theoretical Parker spiral where the radial and transverse components are given as

$$B_r \propto \cos\theta (R/R_0)^{-2}$$
$$B_\phi \propto \sin\theta (R/R_0)^{-1} \qquad (11)$$

respectively. Here θ is the angle between $\mathbf{B}$ and $\mathbf{u}$ for which

$$\tan\theta = \omega_s R_0 / u \qquad (12)$$

with $R_0 = 1AU$ and the solar rotation period $\omega_s \doteq 24.47$ days. For our selection of representative solar wind speeds this implies that $\theta \approx 47°$ and $\theta \approx 31.5°$ for slow and fast wind, respectively. Finally, the proton temperature radial profiles required for computation of $Q_{C,ep}$ in equation (6) are taken from *Hellinger et al.* [2011, 2013].

The resulting heating rates for the isotropic energy balance equations (5) and (6) are shown in Figure 2. The upper panels show both the total heating rate Q and the three individual contributions Q_T, Q_q, and $Q_{C,ep}$ as the function of the radial heliocentric distance for the slow wind (left panel) and fast wind (right panel) separately in a symmetric semi logarithmic scale. Qualitatively, the both cases are similar to each other. The expansional term Q_T (dotted line) stays positive all along the solar wind expansion well in agree-

ment with the observed electron temperature gradient (for an adiabatic radial expansion $T \propto r^{-4/3}$, while observations show T between $r^{-0.3}$ and $r^{-0.7}$ which would imply an additional heating, i.e., a positive Q in our convention) and in turn the heat flux term Q_q (dashed line) provides a negative contribution to the total heating rate Q. As expected, due to a relatively very low frequency of the electron-proton collisions the contribution of $Q_{C,ep}$ term (dash-dotted line) is negligible. The total heating rate Q (solid line) is then given as a competition between the heating required by the adiabatic term and cooling resulting from the significant electron heat flux degradation. In the slow wind the heat flux effect is slightly stronger than in the fast wind and thus the total heating rate in the slow wind is found to be negative indicating that an additional cooling of electrons is required to obtain the observed temperature gradient. In the average fast solar wind the total heating rate is still negative, however, the two terms Q_T and Q_q almost balance each other and the equation (1) is very close to be satisfied without a need of any significant external heat sources or sinks. In Figure 2 we further plot with grey shaded areas the 95% confidence intervals of the total heating rate Q as derived from the error propagation analysis by taking into account the uncertainties of the fitted parameters given in Table 1. Details on the error analysis are given in Appendix B.

In order to remove the radial trends, given by the characteristic density and temperature gradients, from the average
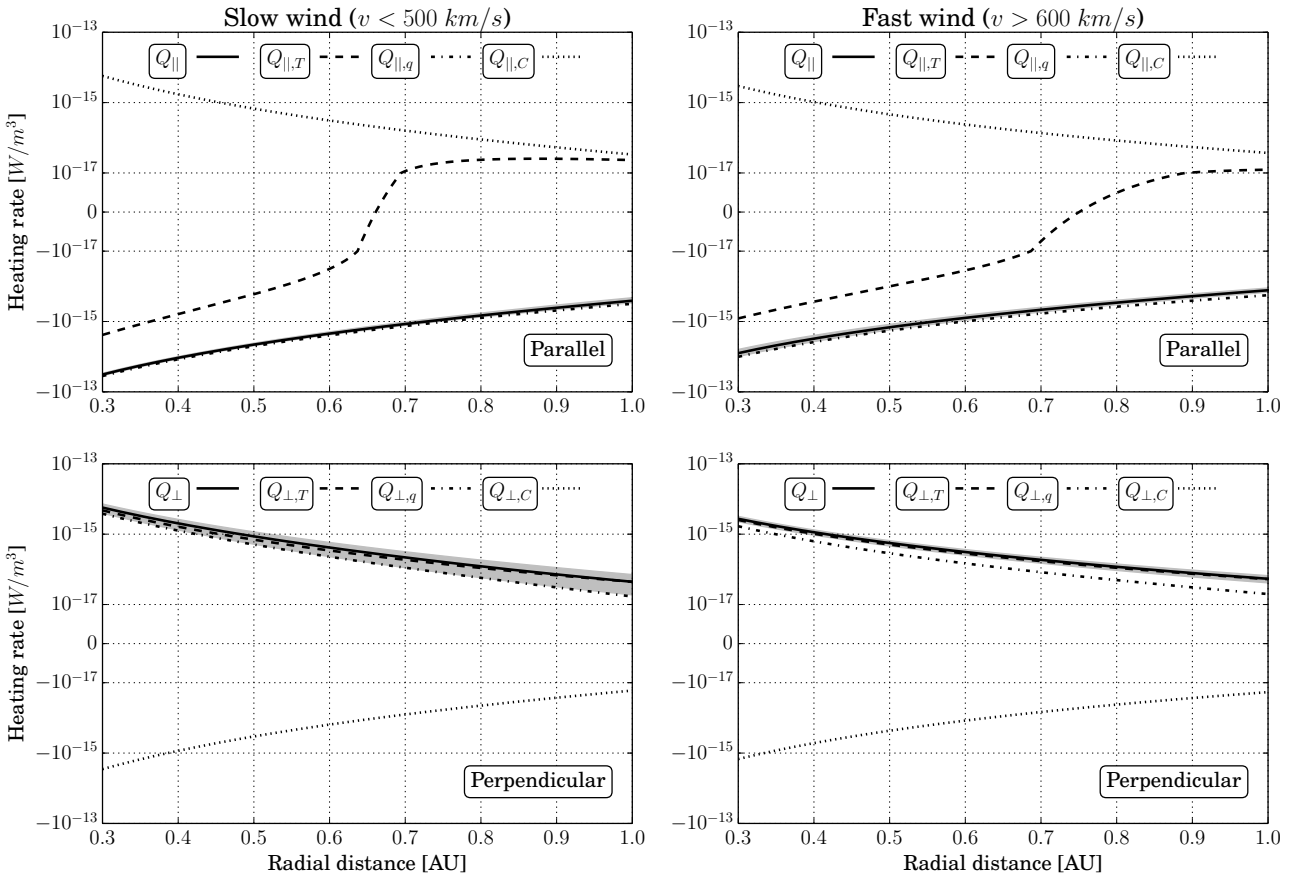
Figure 3. Individual heating rate terms of the anisotropic energy balance equation defined in equations (9) for the parallel direction (upper panels) and equations (10) for the perpendicular direction (lower panels) in the case of slow solar wind (left panels) and fast solar wind (right panels) conditions are shown in W/m^3 as a function of the radial distance from the sun. For each of the two directions the three individual contributions $Q_{.,T}$, $Q_{.,q}$, $Q_{.,C}$ and the sum of them $Q_.$ are represented by dashed, dash-dotted, dotted, and solid line, respectively. The y-axis corresponding to the heating rates employs a symmetric logarithmic scale (with a small linear scale interval around zero). Grey shaded areas identify the 95% confidence intervals.

rate Q and also to better quantify the significance of the derived heating rates the lower panels of Figure 2 express the same quantities normalized to a characteristic rate

$$Q_E = \frac{nk_BTu}{R} \qquad (13)$$

simply given as the ration of the electron internal energy $\approx nk_BT$ and the expansion time R/u. Assuming a negligible heat flux and collisionless plasma we find from the equation (1) the total heating rate Q to be directly proportional to $\propto nk_BTu/R$ and Q_E may therefore serve as a characteristic measure of the relative importance of the derived heating rates [cf., *Hellinger et al.*, 2013]. The normalized quantities are shown in the lower panels of Figure 2 where the lines have the same meaning as in the upper part of the figure. The normalization confirms the significance of both terms Q_T and Q_q and also the resulting cooling effect in the slow wind and rather energetic equilibrium in the fast wind case.

In comparison to the isotropic approach a closer approximation of the true solar wind state, where electron temperatures are typically observed to differ in directions parallel and perpendicular to the local magnetic field lines, should be provided by the equations (7)-(10) where such temperature anisotropy is considered. The corresponding results are shown in Figure 3 and 4. For the rather complex anisotropic approach we first show in Figure 3 the results for the evaluation of equations (8) together with the individual contribu-

tions defined in equations (9) and (10), again expressed as a function of the radial distance where the y-axis employ a symmetric logarithmic scale (with a small linear scale interval around zero) which separates the negative and positive rates. The two columns in Figure 3 are organized so that the left and right panels show the results for slow and fast wind, respectively, while the upper panels show the parallel and the lower panels the perpendicular components of the three individual contributions $Q_{.,T}$, $Q_{.,q}$, $Q_{.,C}$ to the average heating rate $Q_.$ (here the dot in the subscripts is a substitute for either the parallel or perpendicular direction with respect to the ambient magnetic field), the latter terms are represented by dashed, dash-dotted, dotted and solid lines, respectively. Using again the error propagation method described in Appendix B we plot with grey shaded areas the 95% confidence intervals of the total heating rates for both the parallel and perpendicular direction. The two cases, i.e., the slow and fast solar wind representations, indicate qualitatively very similar behavior to each other with negative and positive total heating rates in the parallel and perpendicular directions, respectively. While in the parallel direction the cooling rate $Q_\parallel$ is mainly due to a substantial degradation of the parallel electron heat flux the perpendicular heating rate $Q_\perp$ is mostly provided by the adiabatic expansion term and the perpendicular heat flux and collisional terms almost balance each other. Similarly to results derived for solar wind protons [*Hellinger et al.*,
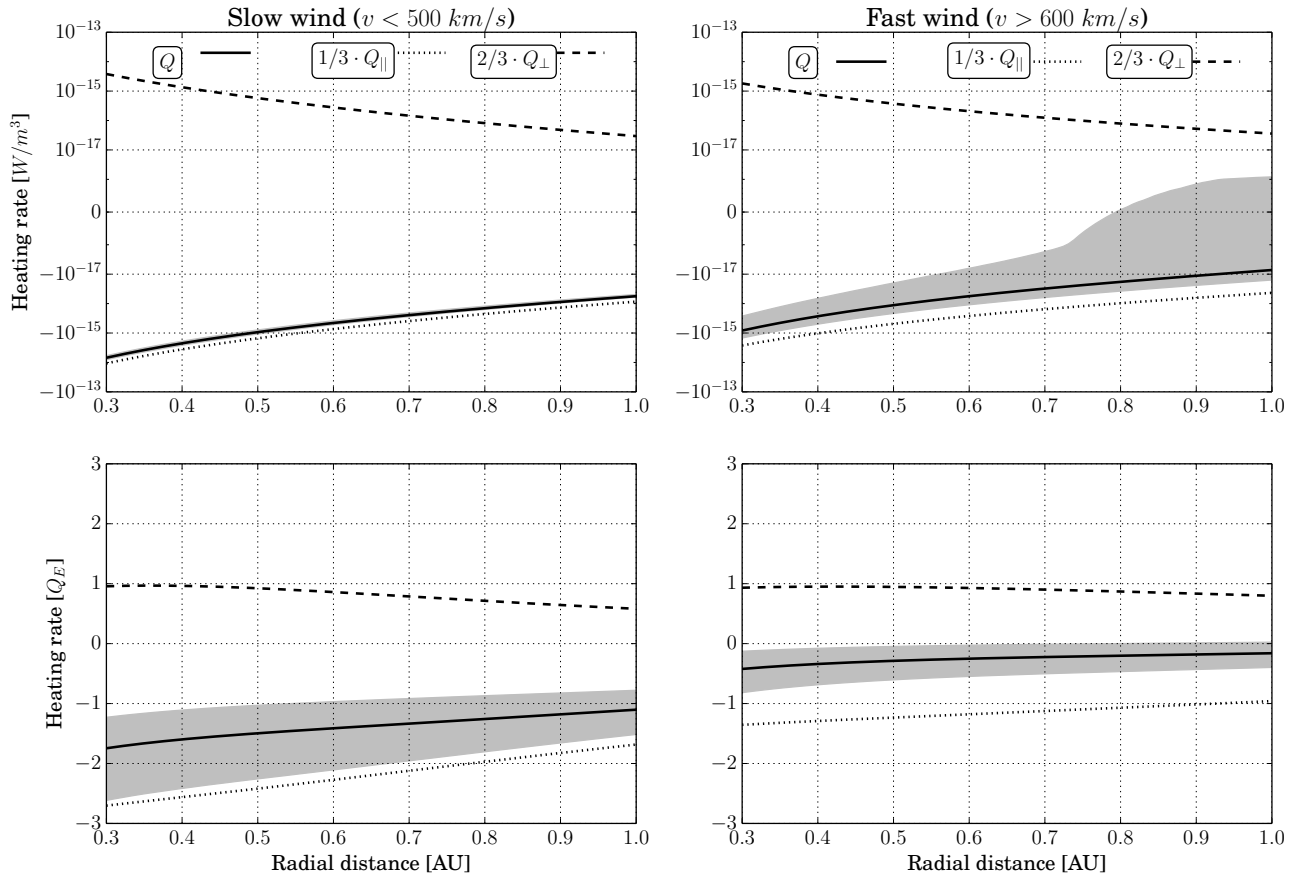
Figure 4. The total electron energy balance derived from the parallel and perpendicular cooling/heating rates are shown in the slow (left panels) and fast solar wind (right panels) for the anisotropic approach. The parallel and perpendicular rates $Q_\perp$, $Q_\parallel$ (see eq. 8) and the total average rate Q are represented by dashed, dotted, and solid lines, respectively. Similarly to previous figures the y-axis in the upper panels corresponds to the heating rates in W/m^3 and employs a symmetric logarithmic scale (with a small linear scale interval around zero). The lower panels show the heating rates normalized to the characteristic heating rate $Q_E = nk_BTu/R$. Grey shaded areas identify the 95% confidence intervals of the total heating rate Q as derived from the error analysis.

2011, 2013] the adiabatic expansion term for the parallel direction changes its sign from being negative closer to the Sun to become positive when approaching 1 AU. Coulomb collisions in the anisotropic approach represent the thermal relaxation of the temperature anisotropy and resulting collisional terms are found comparable (and thus not negligible) in magnitude to the adiabatic and heat flux terms.

The average heating rates Q derived for the anisotropic approach given by the equation (7) are summarized in Figure 4. The upper panels show parallel and perpendicular contributions (dotted and dashed lines) to the total average heating rates (solid line) given in the volumetric units on a symmetric logarithmic scale as a function of the radial distance from the Sun. The lower panels show the same quantities normalized by the characteristic heating rate Q_E. With direct analogy to Figures 2 and 3 we again plot with grey shaded areas the 95% confidence intervals of the total heating rate Q. In the anisotropic approach the total heating rates are presented as a competition between the observed parallel cooling and perpendicular heating. Since the parallel cooling dominates for both the slow and fast solar wind streams we find that the total average heating rate is negative, similarly to the isotropic approach. Still the total average rate in the fast wind is again rather small in agreement to our findings for the isotropic approach. However, the quantities normalized by Q_E show that in the anisotropic

approach the resulting cooling in the fast wind is not completely negligible.

Our data analysis is completed with a comparison between the electron average heating rates and the proton average heating rates derived by *Hellinger et al.* [2011] and *Hellinger et al.* [2013] for solar wind protons. The comparison is shown in Figure 5 for the slow (solid lines) and the fast (dashed lines) solar wind where the upper panel shows a comparison of the electron cooling rates (negative range) and proton heating rates (positive range) per unit volume while in the lower plot we show their relative ratio. The comparison indicates that the Helios observations show the electron cooling rate to be almost ten times higher than the proton heating rate around 0.3 AU and this ratio decreases with radial distance down to a factor of about 4 at 1 AU. For the fast solar wind the radial profile of the ratio $|Q_E/Q_p|$ is rather flat in the observed radial range with $|Q_E/Q_p|$ being about 0.35 at 0.3 AU and going down to roughly 0.3 at 1 AU.

For both the isotropic and anisotropic approach we see that even for relatively small uncertainties in the radial profiles obtained from our large data set the confidence intervals of the resulting heating rates are rather significant with the thickness of the intervals typically ranging roughly between 0.2 and 0.8 when expressed in the normalized units of Q_E. The thick confidence intervals thus indicate a quiet high sensitivity of the heating rates already for even small

perturbations of the input radial profiles. In order to better illustrate the sensitivity of the total heating rates to initial radial profiles we took three different levels of artificial relative uncertainties, namely $\sigma = 1\%$, 5%, and 10%, equal for all the radial profile parameters and derived the corresponding confidence intervals of the average heating rates in the anisotropic approach. In Figure 6 we show the difference between the average heating rate Q and the limits of the confidence intervals Q_{CI} given in Q_E for all three levels of uncertainty in case of both slow (left panel) and fast (right panel) solar wind streams. While for our data set we found the thickness of the confidence intervals to be typically less than one Q_E, Figure 6 shows that the thickness can exceed a few Q_E already for an overall uncertainty of 5%. With respect to these findings we have to remind that we do not assume in our analysis any potential systematic errors, provided for example by the measurement technique itself or by incorrect calibration, which can easily reach several per cents or even more.

3. Discussion

We tested the observed overall energy balance of the electron population in the expanding solar wind based on the second order moment of the Boltzmann equation assuming first the isotropic temperature approach and second a more general anisotropic temperature approach. The energization rates were evaluated not for individual measurements but
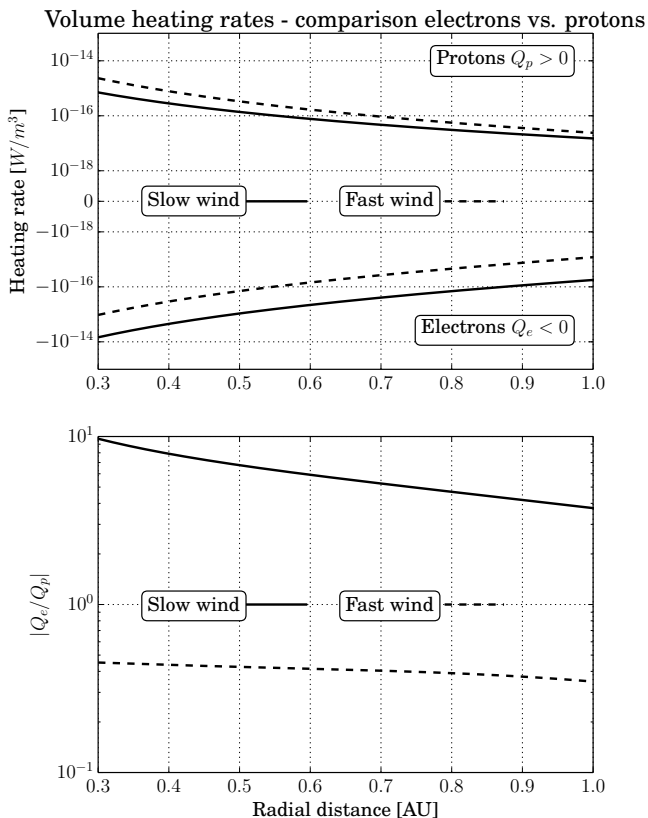

Figure 5. The comparison between the derived electron cooling rates and the proton heating rates (as derived in *Hellinger et al.* [2011, 2013]) required to explain the observed temperature profiles. The upper panel shows the quantities in W/m^3 while the lower panel shows their absolute ratio for both the slow (solid line) and fast solar wind (dashed line).

using mean values of electron macroscopic characteristics represented by empirical radial power-law profiles and by a simple Parker spiral model used to represent the interplanetary ambient magnetic field. We further assumed stationary radial expansion with a constant solar wind speeds. In general, our findings on the heating/cooling rates do therefore rather correspond to a kind of model solar wind having mean observed electron properties at each radial distance which is not fully comparable to the true solar wind having a large range of initial states and expanding under time variable conditions into the heliosphere.

The empirical radial profiles used in our study are summarized in Figure 1. The radial evolution of the electron density in the slow solar wind is found to decrease as $n \propto r^{-2.03}$. Such profile well corresponds to the theoretical stationary radial expansion and supports our assumption of using a constant velocity for evaluation of the heating rates. In the fast wind we find, however, a slightly flatter radial profile of $n \propto r^{-1.83}$ which would correspond to a plasma compression in a decelerated radial expansion. It is important to note that the correction method of measured distribution functions used in *Štverák et al.* [2009], namely the estimation of the spacecraft potential, is based on measured ion density. Indeed, similar radial profile was found for fast solar wind protons by *Hellinger et al.* [2011] where the authors argue that such observational result is compatible with deceleration of the fast wind streams on the slow solar wind in the compression regions. Nevertheless, instead of the corresponding decelerating velocity profile (i.e., $u \propto r^{-0.17}$) we still assume a constant velocity even in the fast wind case in order to keep the model rather simple and comparable with the slow wind case. Yet we verified that the decelerating velocity profile has only a minor effect and does not change qualitatively the resulting total heating rates. The limited effect of the possible variability of the solar wind speed with radial distance is further confirmed by the confidence intervals where the solar wind speed was varied with a standard deviation of 50 km/s (see Appendix B).

The electron temperature and heat flux radial profiles from Helios measurements were originally presented by *Pilipp et al.* [1990] where the bulk electron properties were estimated by direct numerical integration of the measured distribution functions. Although we use a different method to estimate the bulk electron properties, the derived empirical profiles in the slow wind are rather similar (almost identical in temperatures) to those derived in *Pilipp et al.* [1990] (c.f. Figure 3 and Figure 4 therein). The profiles derived in the fast wind slightly differ being in between those presented in *Pilipp et al.* [1990] for high speed streams and compression regions. We did not make any detailed analysis of the fast wind data set assuming that both free high speed streams and also compressed streams (as also indicated by the derived density profile) are present which may explain the observed differences. Differences between radial profiles derived in the present study and those published by Pilipp et al. may be also due to data set restrictions described in section 2.1 and the original data set used by Pilipp et al.

The comparison with radial profiles used in *Cranmer et al.* [2009] is not so straightforward. *Cranmer et al.* [2009] assumed the isotropic approach in the fast solar wind and evaluated only the total electron temperature and total electron parallel heat flux, in our notation these correspond to T and q respectively. Furthermore the fits of the radial empirical profiles used by *Cranmer et al.* [2009] take a more general form as $\ln y = a + b \ln r + c(\ln r)^2$. For a comparison with the simple power-law profile $y = Ar^\alpha$ the local value of α can be evaluated as $\partial \ln y / \partial \ln r$. From equations (2) and (3) in *Cranmer et al.* [2009] we find the α_T to increase from about -0.6 at 0.3 AU to -0.4 at 1 AU and α_q to increase from about -2.7 at 0.3 AU to -2.1 at 1 AU, cf. with $\alpha_T = -0.31$
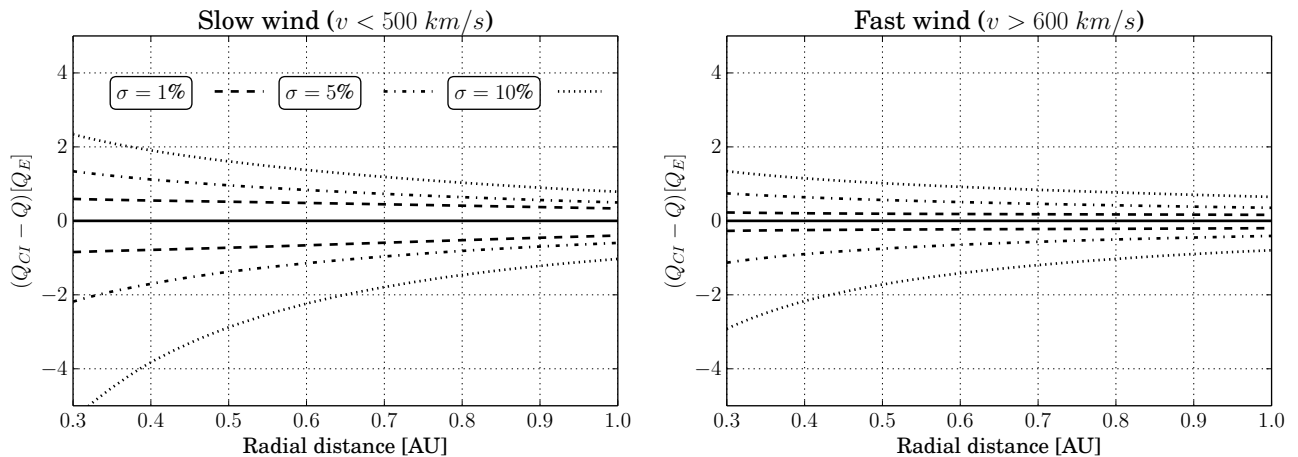
Figure 6. Radius of confidence intervals of total average heating rates in the anisotropic approach are shown for three different uniform levels of artificial radial profile uncertainties, $\sigma = 1\%$ (dashed line), 5% (dash-dotted line), and 10% (dotted line)

and $\alpha_q = -2.44$ given in Table 1 of the present paper. While the comparison for the heat flux gradient is acceptable this is not the case for the electron temperature. Here we have to point out the problematic data set used by *Cranmer et al.* [2009] where the temperature profile is highly affected by a significant bifurcation in the Ulysses data range and so the comparison with our results is rather questionable.

The derived heating rates computed from the mean radial profiles are summarized in Figure 2 and 4 respectively. In general we do not observe any significant qualitative differences between the total average heating rates derived either in the isotropic or the anisotropic approach. In the slow solar wind the normalized average heating rates are significantly negative, which would indicate that the electrons lose the thermal energy in addition to the adiabatic cooling provided by the expansion. The heating rate is found still negative but much less significant in the fast wind showing equations (1) or (2)-(3) respectively nearly to be satisfied without a need for any important external mechanisms. For both the slow and fast solar wind streams the obtained results thus do not indicate any additional heating to be required in order to explain the observed temperature gradients. The considerably stronger cooling rate in the slow wind may be attributed to different radial gradients of the electron heat flux. While in the fast wind the electron heat flux decreases as about $q \propto r^{-2.4}$ the decrease in the slow wind is much steeper with $q \propto r^{-2.8}$ (see Table 1). Consequently, the heating provided by the heat flux gradient is significantly stronger in the slow wind while the cooling resulting from the expansion is rather comparable for both the slow and fast wind streams (see the rates Q_q and Q_T in Figure 2). The different electron heat flux gradients further indicate higher efficiency of the heat flux dissipation in the slow wind compared to fast wind streams. Such hypothesis may be also supported by the recent observations of *Lacombe et al.* [2014] in which they found increased whistler activity most plausibly corresponding to the whistler heat flux instability threshold typically in slow solar wind streams. In case of temperature anisotropy it has been also further shown by *Štverák et al.* [2008] that again slow solar wind electrons are effectively constrained by the corresponding kinetic instabilities while the fast wind is typically observed far away from the instability tresholds.

In a qualitative comparison with previous results we find a good agreement in the slow solar wind with the results of *Pilipp et al.* [1990]. By integration of the total heating rate Q given in equation (7) from 0.3 up to 1 AU *Pilipp et al.* [1990] (cf. eq. (C1) therein) found the total heat required along the expansion to be negative and thus also indicating

external energy sinks rather than any heating sources to be required. In case of sector boundaries and compression regions the total heat was found only slightly higher than zero and thus not fully corresponding to our findings neither in the slow and fast wind. Still, these results may have similar interpretation as ours for the fast wind indicating that external heat sources are not important or are negligible in these regions. In case of the high speed streams *Pilipp et al.* [1990] found the total heat to be significantly positive in agreement with *Cranmer et al.* [2009] where the total heating rate was estimated using the isotropic approach only (cf. eq. (9) therein with equations (5) and (6) in the present paper). This will indicate the electrons in the fast wind to be still heated by any external process in contrast to our result. The disagreement between the previous and present findings may results from the fact that in our analysis we do not attempt to distinguish the different types of fast wind including the compression regions or free streamers and rather simply separate the fast solar wind by the bulk speed. It is also not fully clear how much the resulting electron heating rates in *Cranmer et al.* [2009] are affected by the electron temperature bifurcation in the Ulysses radial range.

In comparison to previous studies we present both the isotropic and the anisotropic approach enabling two different views on the problematic of the electron energetics in the solar wind. The isotropic approach, which neglects the different temperature typically observed in the solar wind in parallel and perpendicular direction wrt. the ambient magnetic field, is summarized in Figure 2. Since the Coulomb electron-proton collisions are shown to be negligible, the overall heating rate may be interpreted as a simple competition of the acting adiabatic cooling due to the solar wind persistent expansion with the heating provided by the dissipation of the electron heat flux. While in the slow wind the heat flux term dominates the adiabatic cooling, the latter two mechanisms almost equally balance each other in the fast wind so that the external energization term Q in equation (1) can be consider for the fast wind as negligible.

The anisotropic approach, representing a closer approximation of the true solar wind state, provides another view on the solar wind energetics. While in the isotropic approach the total rate Q is simply derived from the adiabatic expansion and degradation of the heat flux the anisotropic approach rather defines the total energization rate Q as a mutual energy exchange between the parallel and perpendicular directions. This energy exchange is presented in Figure 4 showing the individual parallel cooling ($Q_\parallel < 0$) and perpendicular heating ($Q_\perp > 0$) rates. Similar to the

isotropic approach the total heating rate is found to be significantly negative in the slow wind with the parallel cooling mechanisms being dominant over the perpendicular component and the latter two are rather close to each other in magnitude for the fast wind case so that the total heating rate is still negative but much less significant. The heating rates derived in the anisotropic approach clearly indicate presence of efficient mechanisms responsible for energy transfer from the parallel to the perpendicular direction. The observed parallel cooling and perpendicular heating also likely represents a macroscopic equivalent of the diffusion of strahl electrons to the halo indicated by observations of *Maksimovic et al.* [2005] and *Štverák et al.* [2009].

Looking more in detail at the individual terms of the parallel and perpendicular heating rates shown in Figure 3, we observe that in contrast to solar wind protons [*Hellinger et al.*, 2011, 2013] both the contribution of the electron heat conduction $Q_{.,q}$ and heating provided by the electron-electron Coulomb collisions $Q_{.,C}$ can not be neglected in comparison to the adiabatic term $Q_{.,T}$. In the parallel direction the heating rates are in fact dominated by a negative contribution of the strong electron heat flux term $Q_{\parallel,q}$. The collisional term $Q_{\parallel,C}$ is found to be positive along the whole observed radial range as $T_\parallel$ is typically greater than $T_\perp$ due to the strahl population. The adiabatic term $Q_{\parallel,T}$ starts as negative at 0.3 AU and later it changes the sign between 0.6-0.7 AU and 0.7-0.8 AU in case of the slow and fast wind respectively. Similar behavior was found for solar wind protons in *Hellinger et al.* [2011, 2013]. The overall parallel heating rate $Q_\parallel$ is found to be negative along the observed radial range which indicates a parallel cooling. In the perpendicular direction the overall heating rate $Q_\perp$ is found positive mainly due to the adiabatic term $Q_{\perp,T}$. The collisional term $Q_{\perp,C}$, symmetric in sign by definition to $Q_{\parallel,C}$ and thus negative in the perpendicular direction, is more or less balanced with positive contribution of $Q_{\perp,q}$.

In general we find the average heating rates in both the slow and fast wind to be negative indicating that instead of being heated the electrons rather lose their thermal energy. The mechanisms providing the additional loss of energy in addition to the adiabatic cooling, dissipation of the electron heat flux, and effect of Coulomb collisions are, however, hardly to be better understood and identified based on the present analysis only. Although it looks problematic to expected any process like the latter mentioned wave-particle interactions or Coulomb collisions to effectively act in the energy transfer back from the electron to proton scales, we also provide a naive comparison of the heat required by protons [*Hellinger et al.*, 2011, 2013] with the average energy being lost by electrons as presented in this paper. Looking at the lower panel of Figure 5 we see that while in the slow wind the amount of the extra energy being dissipated by electrons exceeds the average heating rate required by protons around ten times at 0.3 AU and four times at 1 AU, in the fast wind the dissipated energy represents less than 50% of the one required to heat the solar wind protons. Therefore even if there exists an effective mechanism which may transfer the energy from electrons to protons it won't provide a self-sustaining solution for the heating of solar wind protons along the solar wind expansion.

The critical question of the present analysis is how significant the resulting heating rates are. With the large number of variable parameters in equations (5)-(10) and with their corresponding observational uncertainties, any quantitative statements on the final figures are rather problematic and even the qualitative conclusions shall be taken with caution. Due to a relatively large number of samples in our data set the statistical errors of the mean radial profiles do not exceed a few percents (see Table 1), although the variance of the measured parameters at individual radial distances reach even more than an order of magnitude namely for the

electron heat flux (Figure 1). Taking the statistical errors of the mean radial profiles we derived the confidence intervals of the resulting heating rates showing their thickness to be significant when normalized to the characteristic rate of Q_E. Staying in the confidence limits the results do not change qualitatively in the slow wind and we still find the total heating rates to be significantly negative all along the observed radial range. On the other hand the boundaries of the confidence intervals in the fast solar wind can even reach positive values indicating some external heating mechanisms to be still required (see namely right panels on Figure 2). The rather thick confidence intervals resulting from relatively small uncertainties in the mean radial profiles further indicate a high sensitivity of the heating problem to even small changes in the input parameters. We quantify this effect using an artificial global uncertainty of the input parameters in Figure 6. The thickness of the confidence interval for $\sigma = 1\%$ is almost comparable to our real data set. However, already for $\sigma = 10\%$, a value typically acceptable for rather precise space experimental measurements, the thickness of the confidence intervals rapidly grows up to even several Q_E. Therefore taking into account the plausible systematic (either instrumental or post-processing) errors, neglected in our analysis but often reaching even higher relative uncertainties, can significantly extend the true confidence limits making the interpretation of our analysis and the corresponding conclusions more circumspective.

4. Conclusions

We have presented a detailed statistical analysis of electron energetic properties in the expanding solar wind. In particular, we addressed the fundamental question whether the observed non-adiabatic electron cooling is driven by some external processes or it is rather a direct consequence of mechanisms that exchange and redistribute the internal electron energy. Instead of looking at individual data samples we performed the analysis by constructing two characteristic mean or average solar wind streams as representatives of the distinct slow and fast solar wind populations.

By evaluating the corresponding energy balance equations using the isotropic in comparison to a more general anisotropic approach we found the following conclusions. The observed empirical radial profiles do not indicate any external heat source to be required to explain the temperature gradients for both the slow and fast representative solar wind streams. Actually in the slow wind the results even indicate a significant external cooling to take place. A negative heating rate is equally observed in the fast wind but it is much less significant and, especially in the isotropic approach, it rather shows the fast solar wind to be very close to the energy equilibrium state. In general such different nature of the electron thermal evolution proves the internal energy dissipation mechanisms, very likely provided by wave-particle interactions related to heat flux and/or temperature anisotropy instabilities, to be significantly more effective in the slow than in the fast wind streams.

The detailed analysis of the anisotropic approach shows that all internal mechanisms acting in the energy balance equations are important and can not be neglected. The effect of adiabatic expansion is dominant for the perpendicular heating whereas the dissipation of the electron heat flux is the main driver of the parallel cooling. The importance of Coulomb electron-electron collisions is proven not only by the nominal level of corresponding energization rates, indicating the collisions to represent a very efficient mechanism transfering the internal heat from the parallel to perpendicular direction, but also when comparing the slightly different total rates derived in the isotropic and anisotropic models. Generally instead of asking if any external heating

processes are required for the observed expansion of the solar wind electrons another fundamental question arises, i.e., what are the external sinks of the extra energy being lost due to the electron cooling, namely in the slow solar wind.

We have also investigated the naive question whether the energy lost by electrons would be sufficient to provide the necessary heating rates as derived for solar wind protons by *Hellinger et al.* [2011, 2013]. We found that if there exists an appropriate mechanism for the energy transfer between electrons and protons the electron cooling rate in the slow wind can be sufficient to heat the protons. However, this won't work in the fast wind where the electron cooling is significantly weaker.

In the final remark we point out the statistical uncertainty being present in all above conclusions. We have shown that the electron energetics derived from the energy balance equations is very sensitive to input parameters. In our analysis the relative errors in the empirical radial profiles are very low due to the large data set and so the resulting confidence intervals are still acceptable to confirm qualitatively all the total heating/cooling rates. However, possible important systematic errors, which are not taken into account in our analysis, could modify our findings. Moreover, note that our results do not fully describe the evolution of true observed solar wind streams but rather their mean radial profiles.

Appendix A: Formulary

The definition of all terms used in equations (1) to (13) follows. Here n is the electron number density $n = \int f d^3v$; $\mathbf{u}$ is the solar wind bulk speed; T is the total electron temperature $T = (2T_\perp + T_\parallel)/3$; $T_\parallel$ is the electron parallel temperature $T_\parallel = (m/k_B n) \int v_\parallel^2 f d^3v$; $T_\perp$ is the electron perpendicular temperature $T_\perp = (m/k_B n) \int v_\perp^2 f d^3v$; q is the total electron heat flux $q = (2q_\perp + q_\parallel)/3$, where the two non-zero components of the heat flux tensor are given as $q_\parallel = m \int v_\parallel^3 f d^3v$ and $q_\perp = (m/2) \int v_\parallel v_\perp^2 f d^3v$. In the above definitions m is the electron mass, k_B is the Boltzmann constant, $f = f(v)$ is the electron velocity distribution function in the solar wind frame, i.e., $\int v f d^3v = 0$. The subscripts $\parallel$ and $\perp$ denotes parallel and perpendicular directions with respect to the ambient magnetic field $\mathbf{B}$.

The parallel and perpendicular components of the divergence ∇ are given as $\nabla_\parallel = \mathbf{b}(\mathbf{b} \cdot \nabla)$ and $\nabla_\perp = \nabla - \nabla_\parallel$, where $\mathbf{b}$ is the unit vector of the local background magnetic field $\mathbf{b} = \mathbf{B}/B$.

The collisional terms in equations (1)-(3) are derived based on *Hellinger and Trávníček* [2009] assuming single bi-Maxwellian electron and proton populations only. In the isotropic approach we define

$$\left(\frac{\partial T}{\partial t}\right)_c = \nu_{ep}(T_p - T_e) \quad (A1)$$

where

$$\nu_{ep} = \frac{e^4 n \ln\Lambda}{12\pi^{3/2}\epsilon_0^2 m_e m_p v_{ep}^3} \quad (A2)$$

with e being the elementary charge, $\ln\Lambda$ the Coulomb logarithm, ϵ_0 the free space permittivity, m_e and m_p the electron and proton mass respectively, and $v_{ep} = \sqrt{k_b(T_e/m_e + T_p/m_p)/2}$. The electron temperature T_e is taken from Table 1 and for the proton temperature T_p we use the results derived in *Hellinger et al.* [2011, 2013]. In the anisotropic approach we have

$$\left(\frac{\partial T_\perp}{\partial t}\right)_c = -\frac{1}{2}\left(\frac{\partial T_\parallel}{\partial t}\right)_c = -\nu_T(T_\perp - T_\parallel) \quad (A3)$$

where

$$\nu_T = \frac{e^4 n \ln\Lambda}{30\pi^{3/2}\epsilon_0^2 m^{1/2} k_B^{3/2} T_\parallel^{3/2}} \, {}_2F_1\left(\begin{matrix} 2, 3/2 \\ 7/2 \end{matrix}; 1 - \frac{T_\perp}{T_\parallel}\right) \quad (A4)$$

with ${}_2F_1$ being the standard Gauss hypergeometric function.

Appendix B: Error analysis

When neglecting any systematic errors the uncertainty of the mean radial profiles (4) and its parameters A and α is simply due to the variance between the measurements and the mean (fit) profile, as results from the innate variability of the solar wind properties and random instrumental errors. Since the observed electron properties typically cover at least a few orders of magnitude within the given radial range we estimate this variance using a relative value defined as

$$\sigma_y^2 = \frac{1}{N-1}\sum_N \left(\frac{y_i - \tilde{y}_i}{\tilde{y}_i}\right)^2 \quad , \text{ where } \quad \tilde{y}_i = \tilde{A}(R_i/R_0)^{-\tilde{\alpha}} \quad (B1)$$

here N is the number of individual data samples y_i observed at R_i while $\tilde{A}$ and $\tilde{\alpha}$ are the resulting fit parameters. Consequently, we derive the variance of the model parameters from the error propagation equations [see, e.g., *Bevington and Robinson*, 2003] as

$$\sigma_A^2 = \sigma_y^2 \sum_N \tilde{y}_i^2 \left(\frac{\partial A}{\partial y_i}\right)^2 \quad \text{and} \quad \sigma_\alpha^2 = \sigma_y^2 \sum_N \tilde{y}_i^2 \left(\frac{\partial \alpha}{\partial y_i}\right)^2 \quad (B2)$$

Since our empirical model for the radial gradients is non-linear in parameters we do not have the explicit forms of the parameters as functions of the observed data, i.e., $\tilde{A} = \tilde{A}(y_0, \ldots, y_n)$ and $\tilde{\alpha} = \tilde{\alpha}(y_0, \ldots, y_n)$. Therefore we estimate the partial derivatives in equation (B2) numerically by employing the central differences. The radius of final confidence intervals of the fit parameters is then taken as twice the relative standard deviations, i.e. $\pm 2\sigma_A/\tilde{A}$ and $\pm 2\sigma_\alpha/\tilde{\alpha}$ respectively, see the results listed in Table 1. In general the relative uncertainties of profile parameters are typically less than a few percent. The uncertainties are lower in the slow wind namely due the larger number of data points. The highest uncertainties, with the maximum value of 13% in case of $\sigma_{A,q_\perp}$, are naturally found for the electron heat flux representing a third order moment of the electron velocity distribution function. For comparison and verification we derived the uncertainties from the error matrix as results from the least square fitting and found values very close to those derived by equation (B2).

The uncertainties of all profile parameters naturally affects our estimates of the heating rates. Since all the empirical profiles enter equations (5) to (10) in a rather complex form we have employed a Monte Carlo like error propagation technique. We take the profile parameters as random numbers normally distributed with appropriate σ derived in equation (B2). In addition we take at the same time also the solar wind speed as normally distributed random variable with a standard deviation of 50 km/s which further introduce a variation of the θ angle resulting from the Parker model for the mean interplanetary magnetic field. By taking the random radial profiles we repeat the full evaluation of equations (5)-(10) 100 000 times. Consequently, at each radial distance R we derive the 95% confidence interval by removing the first and last 2.5% data points from the sorted sample of all random results. The resulting confidence intervals for Q, $Q_\parallel$, and $Q_\perp$ are graphically represented in Figures 2, 3, and 4 as grey shaded areas.

References

Barakat, A. R., and R. W. Schunk (1982), Comparison of transport equations based on Maxwellian and bi-Maxwellian distributions for anisotropic plasmas, *Journal of Physics D Applied Physics*, *15*, 1195–1216, doi:10.1088/0022-3727/15/7/014.

Bevington, P., and D. Robinson (2003), *Data reduction and error analysis for the physical sciences*, McGraw-Hill Higher Education, McGraw-Hill.

Bruno, R., and V. Carbone (2013), The Solar Wind as a Turbulence Laboratory, *Living Reviews in Solar Physics*, *10*, 2, doi:10.12942/lrsp-2013-2.

Chew, G. F., M. L. Goldberger, and F. E. Low (1956), The Boltzmann Equation and the One-Fluid Hydromagnetic Equations in the Absence of Particle Collisions, *Royal Society of London Proceedings Series A*, *236*, 112–118, doi:10.1098/rspa.1956.0116.

Cranmer, S. R., W. H. Matthaeus, B. A. Breech, and J. C. Kasper (2009), Empirical Constraints on Proton and Electron Heating in the Fast Solar Wind, *Astrophys. J.*, , *702*, 1604–1614, doi:10.1088/0004-637X/702/2/1604.

Feldman, W., J. R. Asbridge, S. J. Bame, M. D. Montgomery, and S. P. Gary (1975), Solar wind electrons, *J. Geophys. Res.*, *80*, 4181–4196.

Feldman, W. C., J. R. Asbridge, S. J. Bame, and J. T. Gosling (1979), Long-term solar wind electron variations between 1971 and 1978, *J. Geophys. Res.*, *84*, 7371–7377, doi:10.1029/JA084iA12p07371.

Gary, S. P., W. C. Feldman, D. W. Forslund, and M. D. Montgomery (1975), Electron heat flux instabilities in the solar wind, *Geophys. Res. Lett.*, , *2*, 79–82, doi:10.1029/GL002i003p00079.

Gary, S. P., E. E. Scime, J. L. Phillips, and W. C. Feldman (1994), The whistler heat flux instability: Threshold conditions in the solar wind, *J. Geophys. Res.*, , *99*, 23,391–23,399.

Gary, S. P., E. Neagu, R. M. Skoug, and B. E. Goldstein (1999), Solar wind electrons: Parametric constraints, *J. Geophys. Res.*, *104*, 19,843–19,850, doi:10.1029/1999JA900244.

Hellinger, P., and P. M. Trávníček (2009), On Coulomb collisions in bi-Maxwellian plasmas, *Physics of Plasmas*, *16*(5), 054501, doi:10.1063/1.3139253.

Hellinger, P., L. Matteini, Š. Štverák, P. M. Trávníček, and E. Marsch (2011), Heating and cooling of protons in the fast solar wind between 0.3 and 1 AU: Helios revisited, *Journal of Geophysical Research (Space Physics)*, *116*, A09105, doi:10.1029/2011JA016674.

Hellinger, P., P. M. TráVníček, Š. Štverák, L. Matteini, and M. Velli (2013), Proton thermal energetics in the solar wind: Helios reloaded, *Journal of Geophysical Research (Space Physics)*, *118*, 1351–1365, doi:10.1002/jgra.50107.

Hu, Y. Q., R. Esser, and S. R. Habbal (1997), A fast solar wind model with anisotropic proton temperature, *J. Geophys. Res.*, , *102*, 14,661–14,676, doi:10.1029/97JA01040.

Issautier, K., N. Meyer-Vernet, M. Moncuquet, and S. Hoang (1998), Solar wind radial and latitudinal structure - electron density and core temperature from ulysses thermal noise spectroscopy, *J. Geophys. Res.*, *103*, 1969.

Lacombe, C., O. Alexandrova, L. Matteini, O. Santolík, N. Cornilleau-Wehrlin, A. Mangeney, Y. de Conchy, and M. Maksimovic (2014), Whistler Mode Waves and the Electron Heat Flux in the Solar Wind: Cluster Observations, *Astrophys. J.*, , *796*, 5, doi:10.1088/0004-637X/796/1/5.

Landi, S., L. Matteini, and F. Pantellini (2012), On the Competition Between Radial Expansion and Coulomb Collisions in Shaping the Electron Velocity Distribution Function: Kinetic Simulations, *Astrophys. J.*, , *760*, 143, doi:10.1088/0004-637X/760/2/143.

Landi, S., L. Matteini, and F. Pantellini (2014), Electron Heat Flux in the Solar Wind: Are We Observing the Collisional Limit in the 1 AU Data?, *Astrophys. J.*, , *790*, L12, doi:10.1088/2041-8205/790/1/L12.

Maksimovic, M., S. P. Gary, and R. M. Skoug (2000), Solar wind electron suprathermal strength and temperature gradients: Ulysses observations, *J. Geophys. Res.*, *105*, 18,337.

Maksimovic, M., et al. (2005), Radial evolution of the electron distribution functions in the fast solar wind between 0.3 and 1.5 au, *J. Geophys. Res.*, *110*, A09104, doi:10.1029/2005JA011119.

Marquardt, D. (1963), An algorithm of least-squares estimation of nonlinear parameters, *J. Appl. Math.*, *11*, 431–441.

Marsch, E., K. H. Muehlhaeuser, H. Rosenbauer, and R. Schwenn (1983), On the equation of state of solar wind ions derived from HELIOS measurements, *J. Geophys. Res.*, , *88*, 2982–2992, doi:10.1029/JA088iA04p02982.

Montgomery, M. D., S. J. Bame, and A. J. Hundhausen (1968), Solar Wind Electrons: Vela 4 Measurements, *J. Geophys. Res.*, , *73*, 4999–5003, doi:10.1029/JA073i015p04999.

Ogilvie, K. W., and J. D. Scudder (1978), The radial gradients and collisional properties of solar wind electrons, *J. Geophys. Res.*, *83*, 3776–3782, doi:10.1029/JA083iA08p03776.

Pilipp, W. G., H. Miggenrieder, K. H. Muehlhaeuser, H. Rosenbauer, and R. Schuwen (1984), Data analysis of electron measurements of the plasma experiment aboard the HELIOS probes, *NASA STI/Recon Technical Report N*, *85*, 18,935.

Pilipp, W. G., K.-H. Muehlhaeuser, H. Miggenrieder, M. D. Montgomery, and H. Rosenbauer (1987a), Characteristics of electron velocity distribution functions in the solar wind derived from the HELIOS plasma experiment, *J. Geophys. Res.*, , *92*, 1075–1092.

Pilipp, W. G., K.-H. Muehlhaeuser, H. Miggenrieder, H. Rosenbauer, and R. Schwenn (1987b), Variations of electron distribution functions in the solar wind, *J. Geophys. Res.*, , *92*, 1103–1118.

Pilipp, W. G., K.-H. Muehlhaeuser, H. Miggenrieder, H. Rosenbauer, and R. Schwenn (1990), Large-scale variations of thermal electron parameters in the solar wind between 0.3 and 1 AU, *J. Geophys. Res.*, , *95*, 6305–6329, doi:10.1029/JA095iA05p06305.

Rosenbauer, H., et al. (1977), A survey on initial results of the HELIOS plasma experiment, *Journal of Geophysics Zeitschrift für Geophysik*, *42*, 561–580.

Salem, C., D. Hubert, C. Lacombe, A. Mangenay, D. Larson, and L. R.P. (2003), Electron properties and coulomb collisions in the solor wind at 1 au: Wind observations, *Astrophys. J.*, *585*, 1147–1157.

Schulz, M., and A. Eviatar (1973), Validity of CGL equations in solar wind problems, *J. Geophys. Res.*, , *78*, 3948, doi:10.1029/JA078i019p03948.

Schwenn, R., H. Rosenbauer, and H. Miggenrieder (1975), Das Plasmaexperiment auf Helios, *Raumfahrtforschung*, *19*, 226.

Scime, E. E., S. J. Bame, W. C. Feldman, S. P. Gary, J. L. Phillips, and A. Balogh (1994), Regulation of the solar wind electron heat flux from 1 to 5 AU: ULYSSES observations, *J. Geophys. Res.*, *99*, 23,401–23,410.

Štverák, Š., P. Trávníček, M. Maksimovic, E. Marsch, A. N. Fazakerley, and E. E. Scime (2008), Electron temperature anisotropy constraints in the solar wind, *Journal of Geophysical Research (Space Physics)*, *113*, A03,103, doi:10.1029/2007JA012733.

Štverák, Š., M. Maksimovic, P. M. Trávníček, E. Marsch, A. N. Fazakerley, and E. E. Scime (2009), Radial evolution of nonthermal electron populations in the low-latitude solar wind: Helios, Cluster, and Ulysses Observations, *Journal of Geophysical Research (Space Physics)*, *114*, A05104, doi:10.1029/2008JA013883.

Corresponding author: Š. Štverák, Department of Solar Physics, Astronomical Institute, CAS, Prague, Czech Republic. (stepan.stverak@asu.cas.cz)